

# Sensitivity of the C and O production on the $3\alpha$ rate

H. Schlattl ([hs@astro.livjm.ac.uk](mailto:hs@astro.livjm.ac.uk))

*Astrophysics Research Institute, Liverpool John Moores University, Twelve Quays House, Egerton Wharf, Birkenhead CH41 1LD, UK*

A. Heger ([1@2sn.org](mailto:1@2sn.org))

*Department of Astronomy and Astrophysics, University of Chicago, 5640 South Ellis Avenue, Chicago, IL 60637, USA*

H. Oberhummer ([ohu@kph.tuwien.ac.at](mailto:ohu@kph.tuwien.ac.at))

*Atominstytut of the Austrian Universities, Technische Universität Wien, Wiedner Hauptstraße 8–10, A-1040 Wien, Austria*

T. Rauscher ([tommy@quasar.physik.unibas.ch](mailto:tommy@quasar.physik.unibas.ch))

*Departement für Physik und Astronomie, Universität Basel, CH-4056 Basel, Switzerland*

A. Csótó ([csoto@nova.elte.hu](mailto:csoto@nova.elte.hu))

*Department of Atomic Physics, Eötvös University, Pázmány Péter sétány 1/A, H-1117 Budapest, Hungary*

**Abstract.** The dependence of the carbon and oxygen production in stars on the  $3\alpha$  rate is investigated by varying the energy of the  $0_2^+$ -state of  $^{12}\text{C}$  and determining the resulting yields of a selection of low-, intermediate-mass and massive stars. The yields are obtained from modern stellar evolution computations which are following the supernova explosion of massive stars, and considering in detail the 3<sup>rd</sup> dredge-up process during the thermally pulsating asymptotic giant branch of low- and intermediate-mass stars.

Our results show that in massive stars the C and O production is strongly depending on the initial mass, and that it is crucial to follow the whole evolution. The rather strong C production during the He-shell flashes compared to quiescent He burning leads to a lower sensitivity of the C and O production in low- and intermediate-mass stars on the  $3\alpha$ -rate than predicted in our previous work. In particular, the carbon production of intermediate-mass stars seems to have a maximum close to the actual value of the  $0_2^+$  energy level of  $^{12}\text{C}$ .

**Keywords:** stars: abundances – stars: late-type – stars: evolution – stars: interiors

## 1. Introduction

The large binding energy of the  $\alpha$ -particle as compared to its neighbouring nuclei with  $A < 12$  leads to a unique situation. In order to create elements heavier than  $A > 7$  via the fusion of lighter isotopes, high temperatures and high densities would be needed. This already puzzled astrophysics in the middle of the 20<sup>th</sup> century, as under such conditions newly created carbon would almost immediately be fused



© 2019 Kluwer Academic Publishers. Printed in the Netherlands.

further to form heavier elements. As a result, only tiny amounts of carbon would be produced, which is in contradiction to the abundances observed in the universe.

Hoyle et al. (1953) concluded that a then unknown excited state in the  $^{12}\text{C}$  nucleus must exist with an energy close to the  $3\alpha$ -threshold (see also Hoyle, 1954). Through this resonance the probability of the short-living  $^8\text{Be}$  nucleus to capture a further  $\alpha$ -particle would be strongly increased. Indeed, the  $0_2^+$ -state of  $^{12}\text{C}$  has been found experimentally later (Cook et al., 1957), with an energy of  $372 \pm 4$  keV above the ground state of 3  $\alpha$ -particles, close to the predicted value of Hoyle et al. (1953). The modern value of the resonance energy  $E_R^0$  is  $379.47 \pm 0.15$  keV (Firestone et al., 1996).

With the reaction rate of the  $3\alpha$ -process basically being determined only by one resonance, the C-production is crucially depending on the energy level of the  $0_2^+$ -state. For higher resonance energies the ignition of  $3\alpha$ -reactions would be causing essentially all  $^{12}\text{C}$  to be processed further to  $^{16}\text{O}$  under hotter conditions. Reducing the energy level would lead to the consumption of all  $\alpha$ -particles by the  $3\alpha$ -reaction, and thus no  $^{16}\text{O}$  could be created.

Livio et al. (1989) found that the carbon production in intermediate-mass and massive stars is inhibited, if the energy level is increased by about 250 keV, while a 60 keV increase still yields considerable quantities of  $^{12}\text{C}$ . Based on nuclear models, we claimed (Oberhummer et al., 2000, Paper I) that a change of about 0.5% in the strength of the nuclear force or of 4% in the Coulomb force – corresponding to a shift in the  $0_2^+$  energy level of about 130 keV – suffices to inhibit either C or O production in stars.

Recently, Murphy et al. (2001) found indications for a variable fine-structure constant ( $\alpha_F$ ) examining HI 21-cm and molecular QSO absorption lines. According to their analysis  $\Delta\alpha_F/\alpha_F = (-0.72 \pm 0.18) \times 10^{-5}$  for a red-shift range  $0.5 < z < 3.5$ . This would lead to a small alteration in the Coulomb force and thus to modified atomic and nuclear physics during this period. The consequent changes in equation of state, opacity or nuclear reaction rates are, however, too small to alter the evolution of stars considerably, as pointed out by Fiorentini and Ricci (2002).

Although also the resonance energy in  $^{12}\text{C}$  would hardly be shifted by the measured difference in  $\alpha_F$ , there are various circumstances where higher changes in  $E_R^0$  are conceivable: i) in Grand Unified Theories (GUT) the varying fine structure constant would imply that also the coupling constants of the other fundamental forces are variable. For example, the relative change in the QCD scale parameter  $\Lambda$  would be about a factor 30 to 60 larger than the rel-

ative change in  $\alpha_F$  (Langacker et al., 2002, Calmet and Fritsch, 2002, Dent and Fairbairn, 2003)<sup>1</sup>. Depending on the model of the nucleon force the observed value of  $\Delta\alpha_F/\alpha_F$  would then result in a change of up to a few keV in the resonance energy (Oberhummer et al., 2003). ii) it is not clear what kind of time-dependence  $\alpha_F$  is showing, and in particular what value  $\alpha_F$  had during  $z > 3.5$ .

Accounting solely for the uncertainties in GUT and nucleon models, changes in the C and O yields of a few 10% are already not inconceivable, when considering the results of Livio et al. (1989) and Paper I. However, in none of these two works the *full* evolution of the stars was followed. In particular, the exact dredge-up process in low- and intermediate-mass stars was not considered in detail, and later evolutionary stages in massive stars including explosive nucleosynthesis in the supernova and remnant formation (fallback of supernova ejecta) were neglected. In the latter case some O could be produced in neon burning independent of the  $3\alpha$ -rate.

In this work, we follow the evolution of 1.3 and  $5 M_\odot$  stars through their whole asymptotic giant-branch (AGB) evolution using five different values of the resonance energy. The evolutions of 15 and  $25 M_\odot$  stars are followed until onset of core collapse and through the supernova explosion using the standard value of the  $0_2^+$  energy level and cases where it is raised or lowered by 100 keV.

We would like to emphasize, that the changes we consider in the energy of the carbon resonance are not based on the assumption that the experimental resonance energy is not well known. Rather, we assume hypothetical changes in the resonance energy, which may come from, for example, a varying fine structure constant. Our aim is to contribute to the on-going discussions mentioned above by showing what changes in the carbon and oxygen production can realistically be expected in the considered range of energy shift. The comparison with results from galacto-chemical evolution models enables to give first rough limits what variations in the resonance energy are allowed. In addition, our detailed models provide a firmer basis to what extend the carbon and oxygen production in stars is “fine-tuned” in order to create considerable amounts of both elements, which appears to be necessary to enable carbon-based life. In particular, we show that the fine-tuning arguments of Paper I have been considerably weakend.

---

<sup>1</sup> An exception is the model of Chacko et al. (2002), which does not necessarily lead to a change in  $\Lambda$ .

## 2. Stellar input physics

### 2.1. MASSIVE STARS

Models of a  $15 M_{\odot}$  and a  $25 M_{\odot}$  population I stars were calculated using the current version of the implicit stellar evolution code KEPLER (Weaver et al., 1978, Woosley and Weaver, 1995, Heger et al., 2000, Rauscher et al., 2002). A stellar model typically employs of the order of a thousand Lagrangian mass zones that adopt to the structure as needed to resolve gradient or temperature, density, composition, etc. We use the essentially same opacity tables as described below for the intermediate mass stars. Only for temperatures above  $10^8$  K the opacities of Woosley and Weaver (1995) and Weaver et al. (1978) were used. Mass loss by stellar winds is implemented using the rate given by Nieuwenhuijzen and de Jager (1990). Convection (mixing-length theory) and semiconvection were treated as described in Weaver et al. (1978) and Weaver and Woosley (1993) using a time-dependent diffusion approach (see also Woosley et al., 2002, for a recent summary).

For the investigations presented in this paper, we use the approximate 19-isotope network described by Weaver et al. (1978) but include updated nuclear reaction rates (Rauscher et al., 2002). The network includes light isotopes and all  $\alpha$ -nuclei up to  $^{56}\text{Ni}$ , plus Fe isotopes. This is sufficient to trace the change in the C and O abundances throughout all burning stages and for modified  $3\alpha$  rates. Only in the late stages nuclear statistical equilibrium (NSE) and quasi-NSE networks are used to follow the weak interactions in silicon burning and in the iron core in more detail. The networks are directly coupled to the hydrodynamical computation and provide the nuclear energy generation rate in a consistent and energy-conservative way.

It should be noted that He-burning results (and thus also later burning stages) also depend on the  $^{12}\text{C}(\alpha, \gamma)^{16}\text{O}$  rate. It is a well-known and long-standing problem in nuclear astrophysics to determine that rate and its temperature dependence to sufficient accuracy at the relevant temperatures. Despite many efforts, the current experimental accuracy (Buchmann, 1996, Kunz et al., 2001, Kunz et al., 2002) leaves enough room for considerable variation in the rate and the resulting evolution. The effects of an altered  $^{12}\text{C}(\alpha, \gamma)^{16}\text{O}$  rate on the evolution of massive stars were studied in the same approach in Weaver and Woosley (1993), Heger et al. (2002) and Woosley et al. (2003). Nevertheless, it has to be emphasized that the effects of a variation in the  $3\alpha$  rate as investigated here, go by far beyond the change seen in those models. Therefore, we keep the  $^{12}\text{C}(\alpha, \gamma)^{16}\text{O}$  rate fixed here and use 1.2 times the rate of

Buchmann (1996), yielding a cross section of about  $S(300) = 170$  keV barn as recommended by Weaver and Woosley (1993). This treatment is also consistent with recent measurements by Kunz et al., Kunz et al. (2001, 2002).

## 2.2. LOW- AND INTERMEDIATE-MASS STARS

The low- and intermediate-mass stars have been computed with the Garching stellar evolution code (Weiss and Schlattl, 2000), which is able to calculate the evolution through the He flash of low-mass stars (Schlattl et al., 2001, Cassisi et al., 2003b), through the thermally pulsating asymptotic giant branch (TP AGB, Wagenhuber and Weiss, 1994) until the white-dwarf cooling track. Up-to-date input physics was used in the model computations like the OPAL opacities (Iglesias and Rogers, 1996) completed in the low-temperature regime by the tables of Alexander and Ferguson (1994). As equation of state the analytic description of A. Irwin was employed (see, e.g., Cassisi et al., 2003a, for a brief description), which is similar to the OPAL equation of state (Rogers et al., 1996) for solar conditions (see, e.g., Schlattl, 2002), but can be used in a much larger metallicity, temperature and density range. Besides, the temperature gradients in convective regions, the locations of which were defined by the Schwarzschild-criterion, were obtained from the mixing-length theory (Böhm-Vitense, 1958) with the parameter  $\alpha = 1.59$ . For the outer boundary condition of the star an Eddington grey atmosphere has been chosen.

All the major nuclear reactions relevant in the TP AGB evolution to determine the final abundances of C and O are included in the code. The main H-burning reaction rates are taken from Adelberger et al. (1998), while for He burning Caughlan et al.'s (1985) rates are used. The resulting  $^{12}\text{C}(\alpha, \gamma)^{16}\text{O}$ -rate is, in the relevant temperature range ( $0.15 < T/(10^8 \text{ K}) < 0.3$ ), about 20–40% higher than the most recent value of Kunz et al. (2002).

During the standard evolution H- and He-burning are well separated within the star, and therefore two different nuclear networks are applied. In convective regions containing nuclear reactions the chemical evolution is followed by subsequent mixing and burning steps. If, however, H should be engulfed in He-burning regions, both networks are treated automatically in a common scheme, which also incorporates the mixing in convective regions (Schlattl, 1999). For this purpose, a time-dependent mixing approach is used like in the KEPLER code, i.e., the usually assumed instantaneous mixing within convective regions is substituted by a fast diffusive process (Langer et al., 1985).

### 3. Evolutionary stellar models

#### 3.1. MASSIVE STARS

With the KEPLER code (§2.1) we followed the evolution of six models from main-sequence hydrogen burning to the onset of core collapse and through the supernova explosion. For each mass, 15 and  $25 M_{\odot}$ , a complete stellar evolution calculation was performed with the standard  $3\alpha$  rate and two calculations with rates modified by varying the  $0_2^+$  energy level of  $^{12}\text{C}$  by  $\Delta E_{\text{R}} = E_{\text{R}} - E_{\text{R}}^0 = \pm 100 \text{ keV}$ .

##### 3.1.1. *The standard evolution*

A detailed description of the evolution of massive stars can be found, e.g., in Limongi et al. (2000) or Woosley et al. (2002). Here we just provide a brief description of the burning phases.

In the middle panels of Figs. 1 and 2 the evolution of 15 and  $25 M_{\odot}$  stars using the standard value of the  $3\alpha$  rate are shown in a Kippenhahn diagram. The first two convective central burning phases are hydrogen and helium burning. A few 10,000 years after the stars have finished core He burning, carbon burning is ignited producing mainly  $^{20}\text{Ne}$  by  $^{12}\text{C}(^{12}\text{C},\alpha)^{20}\text{Ne}$ , where the  $\alpha$ -particles are captured dominantly by  $^{16}\text{O}$  to form further  $^{20}\text{Ne}$ . Depending on the carbon abundance left by central helium burning, but also by the central entropy which decreases with increasing core size, central carbon burning starts convectively or radiatively. The amount of carbon also determines how extended the shell burning phases are and how long they last. The location of the last carbon shell to persist until core collapse sets the size of the carbon-free core. Larger cores usually allow for bigger iron cores and can decide whether a neutron star or black hole results as remnant.

Only a few 1,000 years after the ignition of C burning, the core temperature reaches values at which  $^{20}\text{Ne}$  is again photo-disintegrating to  $^{16}\text{O}$  (neon burning). The liberated  $\alpha$  particles are consumed to produce  $\alpha$ -nuclei from  $^{24}\text{Mg}$  to  $^{32}\text{S}$ . The next burning phase is oxygen burning, i.e., the fusion of two  $^{16}\text{O}$  nuclei, which results in the formation of nuclei like  $^{28}\text{Si}$ ,  $^{32}\text{S}$ , and  $^{34}\text{S}$  (by additional captures). Central O burning lasts only from a few months to a few years, and is followed by a few hours or days of silicon burning, which is the last burning phase before the core collapse. The latter takes place when the developing iron core has grown sufficiently large. After this, an explosion ensues, likely driven by neutrinos from the hot neutron star (Woosley et al., 2002, Janka et al., 2002). A shock front runs through the stars causing explosive nucleosynthesis. The reaction paths relevant for carbon and oxygen are similar to those in the hydrostatic burning

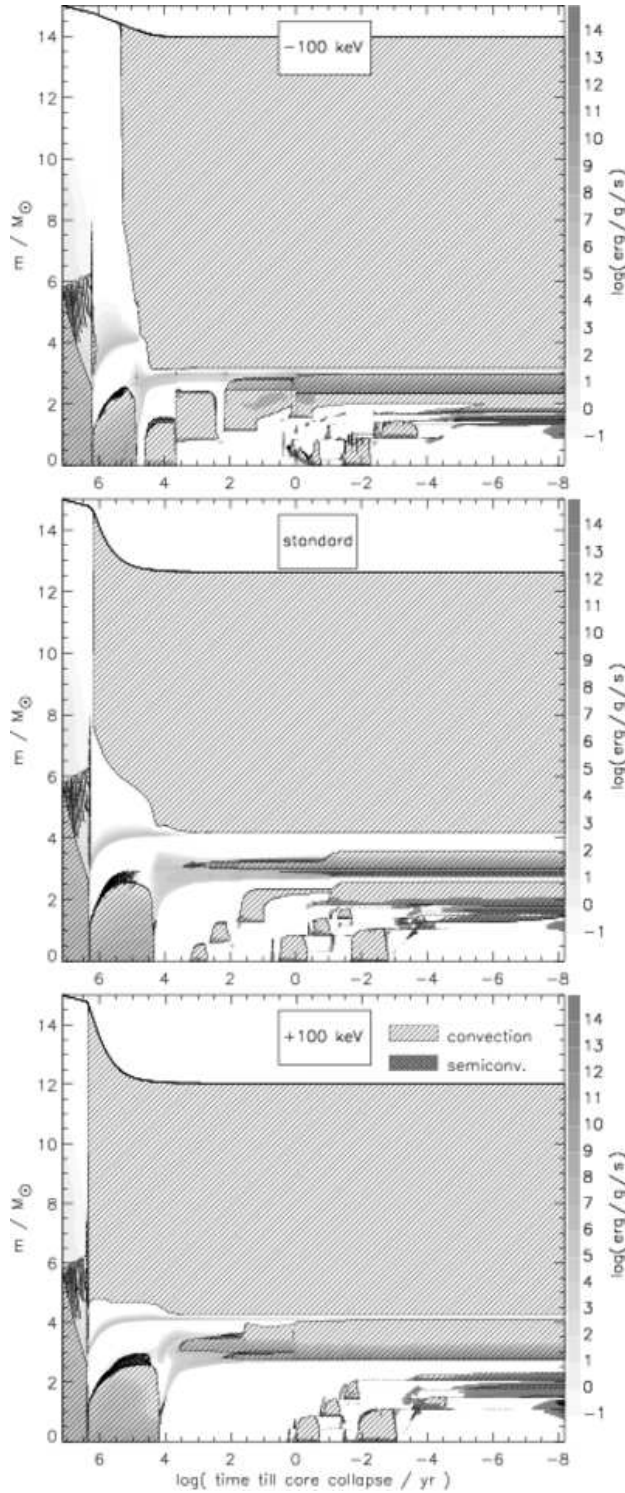


Figure 1. Kippenhahn diagrams of  $15 M_{\odot}$  stars are shown for the three cases:  $\Delta E_R = -100$  (top), 0 (middle), and  $+100$  (bottom). Convective zones are indicated by diagonal hatching and a solid line is drawn around them (the cascade of convective zones above the convective core during hydrogen burning thus appears black). Semiconvection is marked by diagonal cross hatching and the specific nuclear energy generation minus neutrino losses, where positive, by grey shading. The uppermost line indicates the total mass of the star, decreasing due to stellar winds.

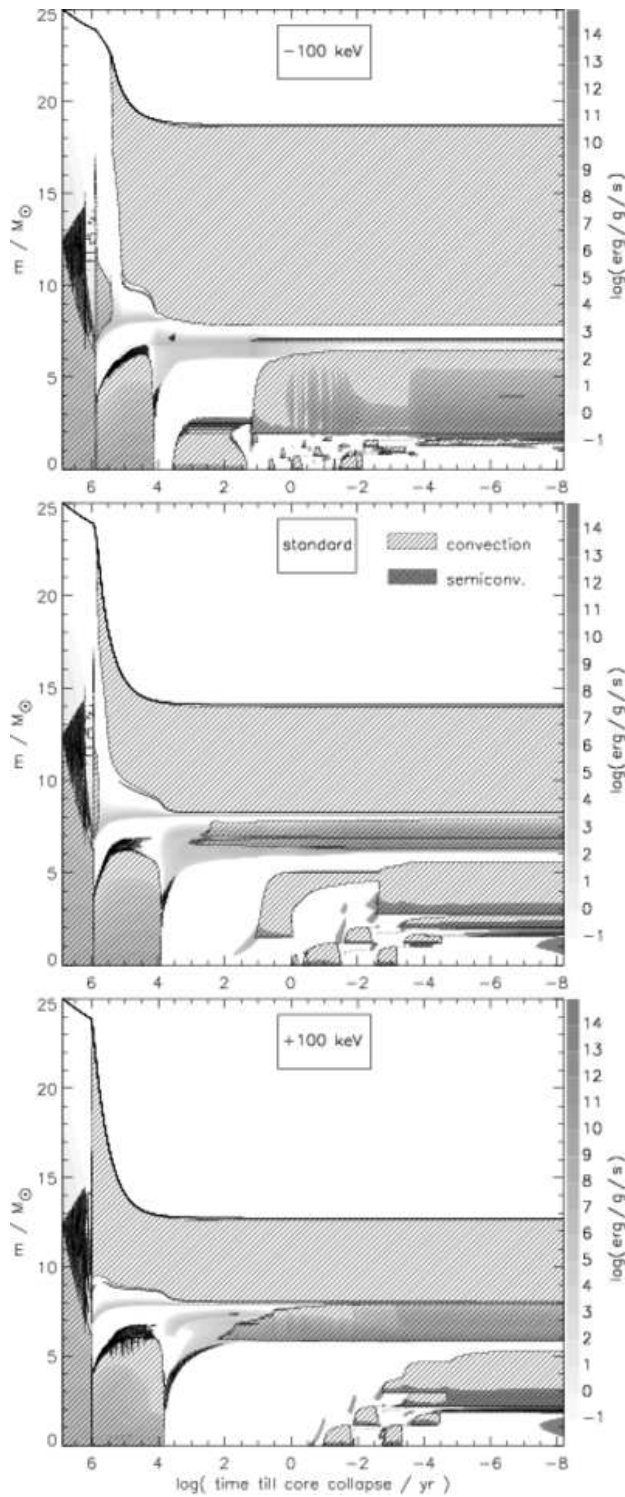


Figure 2. Like Fig. 1 but for  $25 M_{\odot}$  stars.

phases, but occur at higher temperature and on a much shorter time scale.

It must be emphasized that the apparent constancy or only small change in the oxygen mass for the ejecta (Table I) is not a trivial result: Carbon and neon are burnt to oxygen, while oxygen is being burnt to magnesium, silicon and heavier elements.

We simulated the supernova explosion by a piston located at the big rise in entropy usually co-located with the base of the oxygen burning shell, the most likely location for a successful launch of the supernova shock (H.-T. Janka, 2002, private communication). Here, we employed an entropy of  $S = 4 k_B/\text{baryon}$  to place the base of the piston. The piston was first moved inward down to 500 km, accelerating at a constant fraction of the local gravitational acceleration (25% as fit to models by H.-T. Janka and M. Rampp, 2002, private communication). Then it was moved outward to 10,000 km where it reached zero velocity and was stopped. It was decelerated by a different constant fraction of the local gravitational acceleration which was adjusted, together with the initial velocity after the bounce, to match a kinetic energy of the ejecta of  $1.2 \times 10^{51}$  erg (more details will be provided in Heger, A. & Woosley, S. E., in preparation). The amount of mass that was ejected or fell back onto the remnant was then determined by following the hydrodynamical evolution of the supernova and its nucleosynthesis.

The resulting masses of C and O in the stellar ejecta are summarized in Table I. In order to obtain values independent of the initial composition and since we are only interested in the production of new carbon and oxygen, we omitted the amount of C and O in the envelope and we also excluded the inner part of the core that later becomes part of the remnant. That is, the sums given in Table I only comprise the layers with mass coordinates between that of the remnant and the helium core mass given in Table III. It should be noted, that the central evolution of the star and thus the obtained C and O yields in the supernova ejecta are fairly independent of the initial composition (while this is not true for some rarer isotopes like the *s*-process).

Although the CNO cycle does slightly affect the carbon and oxygen yields of massive stars by modifying the envelope content in the 1<sup>st</sup> and/or 2<sup>nd</sup> dredge-up, they would strongly depend on the initial abundance ratio of CNO isotopes as they have been made by earlier generations of massive and intermediate-mass stars. Since we are interested on the effect of different  $3\alpha$  reactions on the yields of certain types of stars, without considering the full chemical history of their initial material, we remove the contribution of initial abundances from our analysis. Note that in the standard case the amount of C and O in the envelope is negligible compared to their abundances in the interior,

Table I. The total mass of C and O in the helium core ejected by the supernova for the 15 and  $25 M_{\odot}$  stars. We only include the masses in the ejecta but disregard the hydrogen envelope (see text) as well as mass in regions that later become part of the remnant. In each of the two sections, the upper rows give carbon and oxygen masses after core helium depletion, the second rows the masses after core carbon burning when a central temperature of  $1.2^9$  K is reached, the third rows that at onset of core collapse and the bottom rows the yields after the supernova explosions.

$\frac{\Delta E_R}{\text{keV}}$	$15 M_{\odot}$			$25 M_{\odot}$		
	-100	0	+100	-100	0	+100
$M_{\text{He}}(\text{C})$	1.05	0.32	0.00	3.69	1.03	0.00
$M_{\text{C}}(\text{C})$	0.38	0.21	0.01	3.11	0.72	0.01
$M_{\text{col}}(\text{C})$	0.36	0.13	0.02	2.65	0.34	0.02
$M_{\text{SN}}(\text{C})$	0.36	0.13	0.02	2.57	0.34	0.02
$M_{\text{He}}(\text{O})$	0.04	0.87	0.46	1.20	3.60	2.11
$M_{\text{C}}(\text{O})$	0.02	0.85	0.46	0.95	3.50	2.04
$M_{\text{col}}(\text{O})$	0.05	0.86	0.48	0.79	3.27	1.84
$M_{\text{SN}}(\text{O})$	0.06	0.71	0.33	0.81	3.09	1.64

but it would influence the results in the case where  $\Delta E_R = -100$  keV. There, in particular the reduction of carbon in the envelope by the CNO cycle is significant compared with the total carbon made.

In contrast to carbon, oxygen is produced in *two* phases of hydrostatic stellar nucleosynthesis: in the helium and in the neon burning. Both C and O are destroyed, in part, in the core by later hydrostatic burning phases. The oxygen abundance is additionally affected by explosive nucleosynthesis while carbon is not changed much by the supernova shock. Therefore, we have provided the carbon and oxygen yields at four stages in Table I: after central helium and carbon depletion, at core collapse, and after the supernova explosion. For central helium depletion we additionally give the central mass fractions of key elements in Table II.

### 3.1.2. Models with $\Delta E_R = -100$ keV

When reducing  $\Delta E_R$ , the ignition of He fusion takes place at lower temperature, where  $^{12}\text{C}(\alpha, \gamma)^{16}\text{O}$  is less efficient. Thus, less oxygen is produced during this phase as shown in detail in Paper I. However, the evolution of the massive stars was followed in Paper I, due to a limited nuclear network, only until the core temperature reached  $10^9$  K, which corresponds to the end of core C burning. Several effects could thus not be accounted for: Firstly, the higher amount of C created in models with  $\Delta E_R = -100$  keV might lead, during C burning, to an enhanced

Table II. Central mass fractions (%) of key elements after core helium depletion for the  $15 M_{\odot}$  and  $25 M_{\odot}$  stars.

$\frac{\Delta E_R}{\text{keV}}$	$15 M_{\odot}$			$25 M_{\odot}$		
	-100	0	+100	-100	0	+100
C	93.03	21.47	<0.01	73.20	19.11	<0.01
O	4.68	76.16	49.76	24.49	78.17	45.41
Ne	1.96	2.03	14.25	1.97	2.33	15.08
Mg	0.07	0.08	35.65	0.08	0.12	39.17
Si	0.08	0.08	0.15	0.08	0.08	0.15
S	0.04	0.04	0.04	0.04	0.04	0.04

Ne production, and thus the O yield of neon burning might be bigger than in the standard case. Secondly, different chemical, temperature and density profiles of the star after core C burning influence the subsequent evolution, leading to different final sizes of the Ne/Mg/O core (abbreviated as ‘Ne/O core’ in Table III) and the Si core, i.e., the amount of carbon and oxygen burnt in the star until it reached core collapse was not determined. Thirdly, oxygen is also destroyed during the explosive burning of the supernova. And last, in case the iron core is too big to make a powerful explosion, a significant part of the oxygen-rich layers may fall back onto the remnant and form a black hole. Here we assumed that all stars resulted in successful explosions with  $1.2 \times 10^{51}$  erg kinetic energy of the ejecta and we obtained no fallback of oxygen or carbon.

To demonstrate the second point, in addition to Figs. 1 and 2, we have shown in Fig. 3 the evolution of central density and temperature. Due to the lower resonance energy, helium burning starts at lower temperature, seen in the lower left corner of the figures. After helium burning, the larger amount of carbon causes more extended and longer-lasting carbon shell burning, followed by well expressed neon burning shells in the  $25 M_{\odot}$  star inside a small carbon-free core, or even off-centre neon ignition (due to high degeneracy) was found in the  $15 M_{\odot}$  star. Indeed, the core of the  $25 M_{\odot}$  star with lowered resonance energy seems to have some similarity with the  $15 M_{\odot}$  standard case. Likely as a consequence of helium burning at higher entropy (higher temperature and lower density), the structure of the star also allows for a dredge-up of the outer layers of the helium core as the entropy step at the edge of the core is decreased. We also note that the modified models spent a significant time of their helium burning as blue stars with radiative envelopes.

Table III. Properties of  $15$  and  $25 M_{\odot}$  stars at the onset of core collapse, where  $M_{\text{preSN}}$  is the final stellar mass. All masses are in units of  $M_{\odot}$ . The last column gives the remnant mass (baryonic mass) including fall back after the supernova explosion assuming a kinetic energy of the ejecta of  $1.2 \times 10^{51}$  erg.

$\frac{\Delta E_{\text{R}}}{\text{keV}}$	$15 M_{\odot}$			$25 M_{\odot}$		
	-100	0	+100	-100	0	+100
$M_{\text{preSN}}$	14.0	12.6	12.0	18.7	14.1	12.7
He core	3.10 <sup>†</sup>	4.10	4.11	7.83 <sup>†</sup>	8.09	7.91
C/O core	2.35	2.77	2.77	6.48	6.26	5.87
Ne/O core	1.72	1.86	2.77	1.84	2.73	5.87
Si core	1.42	1.70	2.05	1.66	2.10	2.85
Fe core	1.42	1.54	1.58	1.64	1.69	1.88
remnant	1.63	1.71	2.05	1.78	2.05	2.19

<sup>†</sup> Helium core mass reduced due to dredge-up.

The final C and O yields of these stars are provided in Table I. In the  $25 M_{\odot}$  star with the lowered resonance energy oxygen is still efficiently destroyed in the hydrostatic burning phases after core helium depletion. In the  $15 M_{\odot}$  star, however, oxygen is even produced. For both masses a small amount of oxygen is made in the supernova explosion. In the  $25 M_{\odot}$  star the carbon shell is so deep inside the star that  $0.08 M_{\odot}$  of C is destroyed there. In this star,  $0.023 M_{\odot}$  of O are made here in explosive carbon and neon burning, while in the underlying Ne/Mg/O layer  $0.001 M_{\odot}$  oxygen is destroyed and only nickel and silicon are made. In the  $15 M_{\odot}$  star  $0.015 M_{\odot}$  of oxygen are destroyed in Ne/Mg/O layer and at the base of the C shell in explosive nucleosynthesis (and a trace at the base of the He shell), but  $0.027 M_{\odot}$  oxygen are made.

### 3.1.3. Models with $\Delta E_{\text{R}} = +100 \text{ keV}$

When the resonance energy is increased, helium burning ignites and proceeds at higher temperature (Fig. 3). At these high temperatures the  $^{12}\text{C}(\alpha, \gamma)^{16}\text{O}$  reaction effectively destroys any carbon made. The core is more compact and more luminous, resulting in a more extended convective red supergiant envelope, developing very rapidly after core hydrogen depletion and exerting higher wind mass loss (Figs. 1 and 2). At the end of helium burning, essentially no carbon is left (Table II). Significant amounts of heavier elements, neon and magnesium are made already in central helium burning. Consequently there is no carbon shell burning that would affect the contraction of the helium-free core. However, neon burning is a well developed convective phase – but now

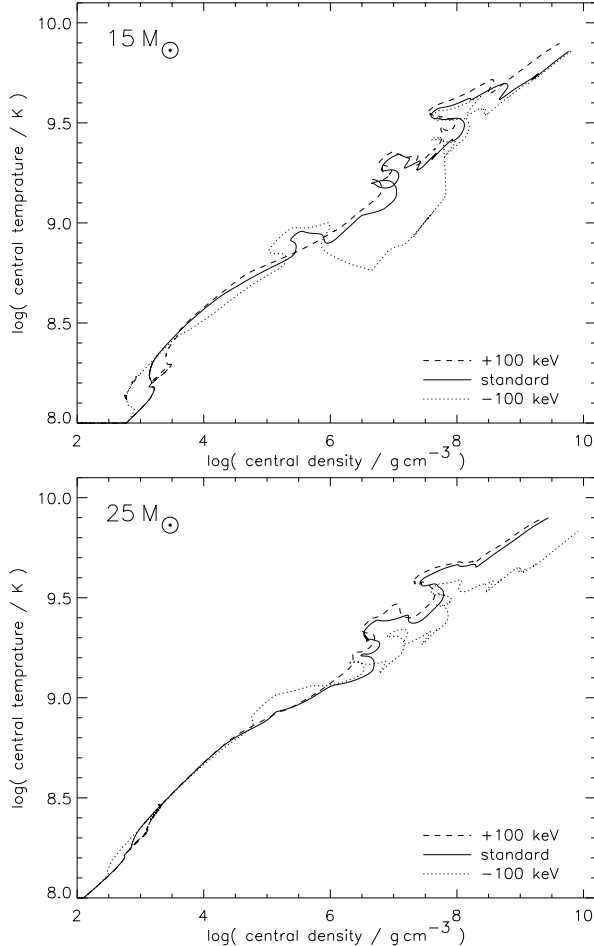


Figure 3. In the upper panel the evolution of central temperature and central density in  $15 M_{\odot}$  stars after hydrogen depletion is shown for the three cases:  $\Delta E_R = -100$  (dotted line), 0 (solid), and  $+100$  (dashed). Generally, massive stars evolve to higher central densities and temperatures, but degeneracy and central and shell burning stages cause several ‘wiggles’ along the way. In the lower panel the same is shown for  $25 M_{\odot}$  stars.

due to neon made in helium burning not due to one made in carbon burning. This is followed by extended central and shell oxygen burning phases, and a big iron core of high entropy results.

In the  $15 M_{\odot}$  star the production and destruction of oxygen is about balanced – oxygen burning is competing with converting the neon made in helium burning into oxygen, slightly favouring its production. Conversely, in the  $25 M_{\odot}$  star the large extent of the oxygen burning shells reduces its yield. In both cases a significant amount of oxygen

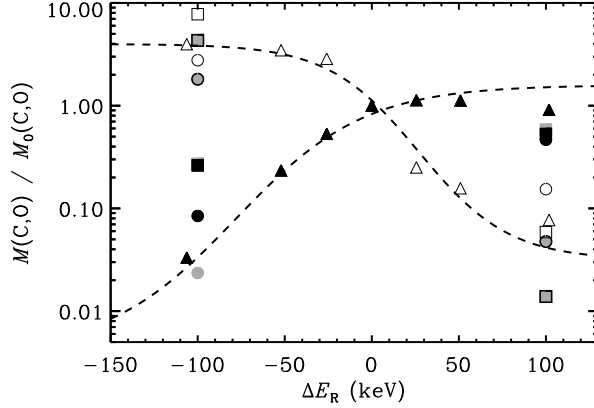


Figure 4. The dependence of the overall amount of C and O produced in massive stars on  $E_R$ . The SN yields of Table I are shown as black O's ( $15 M_\odot$ ) and  $\square$ 's ( $25 M_\odot$ ), where the open and filled symbols denote C and O, respectively, while the yields after core C exhaustion are marked by grey symbols (solid: O, framed: C). For comparison the results obtained in Paper I are shown, too, indicated by open and solid  $\Delta$ 's, where the dashed line has been drawn to guide the eye.

is destroyed in the supernova explosion, but as most of the carbon contained in the helium core is made in the helium-burning shell, its yields are not affected.

### 3.1.4. Summary

In Fig. 4 the change of the C and O production in the  $15 M_\odot$  and  $25 M_\odot$  stars when modifying the resonance energy is shown. Overall the behaviour is similar to what has been found in Paper I, where a  $20 M_\odot$  star has been followed with the Garching stellar evolution code until the end of core C burning. But considering the SN yields, the suppression of C ( $\Delta E_R = 100$  keV) or O ( $\Delta E_R = -100$  keV) is smaller than predicted in Paper I. In particular, the O yields in the  $25 M_\odot$  star for  $\Delta E_R = 100$  keV are only diminished by about a factor of 4, while in Paper I an almost one order of magnitude higher reduction was predicted. In the few models we have computed, there appears to be a tendency of maintaining or creating more C and O after the core C burning for both  $\Delta E_R = -100$  and  $+100$  keV than in the standard case. The post C-burning evolution and the resulting carbon and oxygen yields depend on the extent of the different burning zones and their interaction in the course of late stellar evolution. This can vary strongly as a function of initial mass and thus a trend more along the line of Paper I may result if averaging over a larger set of initial masses (using an initial mass function) were done.

The different results from Paper I compared to the present paper may have several reasons. Firstly, we were employing a different stellar evolution code (KEPLER) than in Paper I (Garching stellar evolution code) which includes a different  $^{12}\text{C}(\alpha, \gamma)^{16}\text{O}$  reaction rate, which is also a key ingredient to the resulting C/O ratio. KEPLER also uses a different treatment of convective boundaries (overshooting) and semiconvection (operating in regions that are stable against convection according to the Ledoux but not according to the Schwarzschild criterion). The latter process has an important role in massive stars. Secondly, our new calculations follow the entire evolution of the star through the supernova explosion and therefore we can determine how much mass falls back on the remnant. For the yields we provide in the present paper (Table I and Fig. 4) we self-consistently excluded this inner region of the star, unlike in Paper I where this information was not available. For comparison, we also calculated the overall yields after core C burning obtained by the KEPLER code. The relative change of the yields when modifying  $E_R$  were, however, not significantly different from the results shown in Fig. 4. So we conclude that most of the discrepancies between Paper I and the present work are indeed caused by the different physics applied.

In any case, the results of this work show that the suppression of C and O in the appropriate case is smaller and depending on the initial mass. Furthermore, it is essential to follow the complete evolution of the star, at least until the pre-collapse phase to obtain reliable results for each stellar mass. The destruction of oxygen by explosive oxygen burning and the production of oxygen by explosive neon burning during the supernova explosion may give non-negligible contributions. In particular the latter may cause that always some oxygen is made, even in the case of rather low  $\Delta E_R$  values. Comparing the yields for the 15 and  $25 M_\odot$  stars before and after the SN explosion (Table I), the minimum amount of O produced could be as high as about  $0.01 M_\odot$ . This would lead to a maximal suppression of the O production for  $\Delta E_R < 0$  of the order of a few 0.1%.

### 3.2. INTERMEDIATE-MASS STARS

We computed sequences of  $5 M_\odot$  stars from the ZAMS to the end of the AGB for 5 different values of the  $0_2^+$  resonance energy in  $^{12}\text{C}$  with the Garching stellar evolution code (§2.2). The initial composition was chosen to be scaled solar with  $[\text{Fe}/\text{H}] = -2.3$ , but as for massive stars, the influence of the initial metallicity on the final C and O production is small for intermediate-mass stars, too.

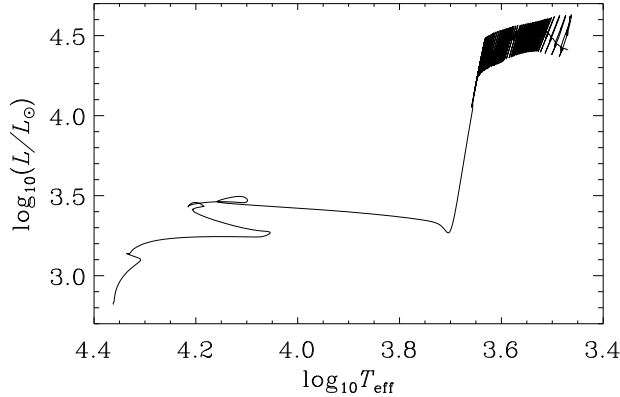


Figure 5. The evolution of a  $5 M_{\odot}$  star in the H-R diagram.

The sequences could not be followed through the final pulse due to a considerable reduction of the gas pressure with a concomitant super-Eddington luminosity. Under this condition the star cannot be treated in quasi-static equilibrium, and thus the models fail to converge. However, the envelope will be removed from the nucleus by radiation, and the remnant will become a white dwarf (Wood and Faulkner, 1986, Faulkner, 1970, Finzi and Wolf, 1971). Thus, by combining the abundances in the wind and in the stellar envelope, a good measure of the total amount of C and O emitted into the inter-stellar medium (ISM) by the stars under scrutiny is obtained.

Mass loss is implemented according to Reimers (1975) with an efficiency parameter  $\eta = 0.8$ . To model the strong winds on the tip of the AGB a description as used, e.g., by Marigo et al. (1996) is applied, which accounts for the mass loss during Mira and super-wind phase (see also Vassiliadis and Wood, 1993).

### 3.2.1. The standard case

In Fig. 5 the evolution of a model with standard  $3\alpha$ -rate is shown with about 50 pulses along the TP AGB. With each pulse the star slowly becomes cooler due to the gradual enrichment of the surface with mainly carbon via the 3<sup>rd</sup> dredge-up, the mechanism of which is outlined in Fig. 6: During the quiescent He-burning phase between 2 pulses, the He shell becomes gradually thinner and thus thermally unstable (see, e.g., Kippenhahn and Weigert, 1990). The increasing energy released within this shell creates a convective zone between the H and He shell (inter-shell convective zone: ISCZ) enriched by He-burning products. Moreover, the He shell and the overlying layers start to expand and

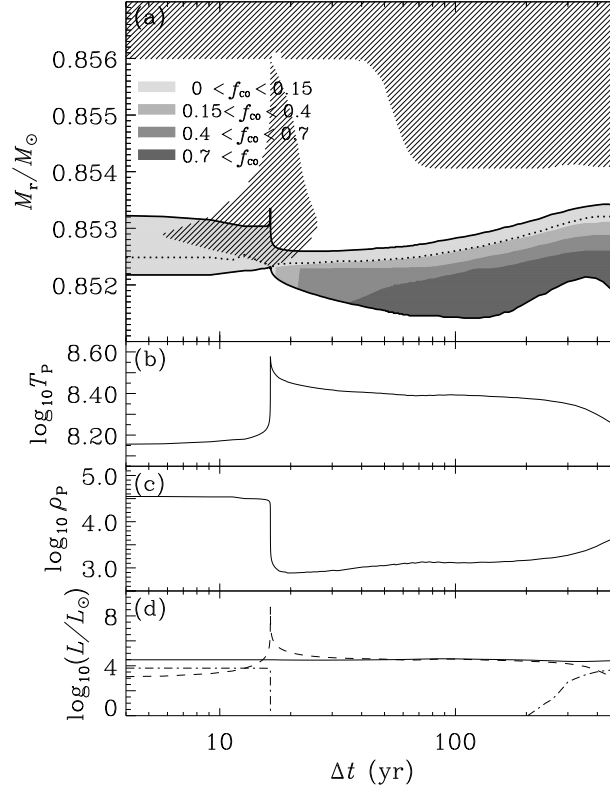


Figure 6. (a) The evolution of convective (hatched areas) and He-burning regions during a thermal pulse. The enclosed grey-scaled area marks the region where 90% of the He-burning energy is released, where each shade of grey indicates the different values of  $f_{\infty}$  (Eq. (3)). The dotted line marks the location of maximum He-burning energy release. (b) The evolution of the temperature at the He-burning energy peak (dotted line in a). (c) The density at the same position. (d) The evolution of the total stellar luminosity (solid line), and the H- (dash-dotted) and He-burning energy output (dashed line).

to cool (Fig. 6b,c), which reduces the H-burning efficiency until it is eventually ceasing (Fig. 6d).

After the He-shell flash the convective envelope deepens overlapping with regions previously occupied by the ISCH, and thus newly created  $^{12}\text{C}$  is mixed to the surface ('3<sup>rd</sup> dredge up'). In the subsequent evolution the outer layers contract, and both H- and He-burning shells are restored, until the latter becomes unstable again, and the next thermal pulse develops.

Since the region of the ISCH is subsequently covered by He- and H-burning reactions, a variety of nuclear processes are taking place including some neutron-producing reactions, which are, in particular

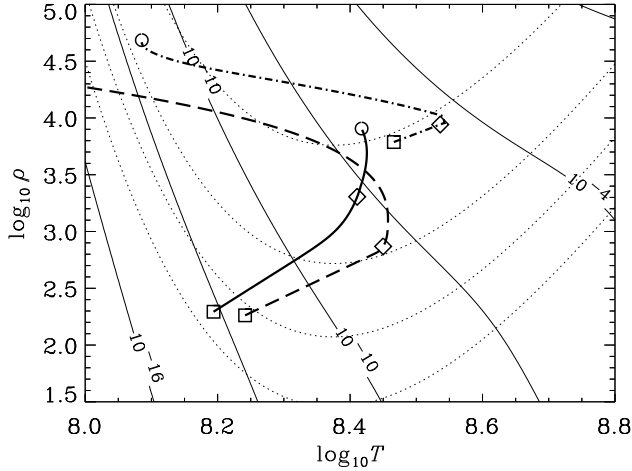


Figure 7. The relative and absolute efficiency of the  $^{12}\text{C}+\alpha$  and  $3\alpha$  reactions. The dotted lines mark the positions of  $f_\sigma^{\text{CO}} = 0.67, 0.33, 0.1$  and  $0.01$  (from bottom to top; Eq. (1)). The thin lines oriented dominantly vertically show equal values of  $\sigma_n^{\text{C}\alpha} + \sigma_n^{3\alpha}$  (in  $\text{g s}^{-1} \text{mol}^{-1}$ ; Eq. (2)), separated in steps of 3 dex, indicating the overall efficiency of He-burning. The thick lines show the stratification of the shell with  $0.8514 < M_r/M_\odot < 0.8534$  at  $\Delta t = 16.4$  (dash-dotted), 20 (dashed) and 95 yr (solid line) (cf. Fig. 6). Equal symbols mark equal mass shells, where  $\square$ ,  $\diamond$  and  $\circ$  are located at  $M_r/M_\odot = 0.8534, 0.8524$  and  $0.8514$ , respectively (cf. Fig. 6a).

in more massive stars, thought to be sufficiently abundant to create elements beyond Fe via the so-called ‘s-process’. However, in this work we are only interested in the final amount of C and O produced, which is much less complicated, and poses less demands on the nuclear network.

The C and O abundances in the ISCZ are crucially depending on the relative strengths of the  $3\alpha$ - and  $^{12}\text{C}+\alpha$ -reaction during the He-shell flash. To illustrate their efficiency inside the star, we have plotted in Fig. 7

$$f_\sigma^{\text{CO}} = \frac{\sigma_n^{3\alpha}}{\sigma_n^{\text{C}\alpha} + \sigma_n^{3\alpha}}, \quad (1)$$

where

$$\begin{aligned} \sigma_n^{3\alpha} &= \frac{\dot{n}_\text{C}}{n_\text{He}^3} = \frac{1}{6} \frac{\varrho}{m_u} \langle \sigma v \rangle_{3\alpha} \quad \text{and} \\ \sigma_n^{\text{C}\alpha} &= \frac{\dot{n}_\text{O}}{n_\text{C} n_\text{He}} = \frac{\varrho}{m_u} \langle \sigma v \rangle_{^{12}\text{C}+\alpha} \end{aligned} \quad (2)$$

with  $n$ ,  $\varrho$ ,  $m_u$  and  $\langle \sigma v \rangle$  being number density, mass density, atomic mass unit and velocity averaged cross section, respectively<sup>2</sup>.

<sup>2</sup> For convenience, the indices He and C denote  $^4\text{He}$  and  $^{12}\text{C}$ , respectively.

The temperature-density stratification between  $M_r/M_\odot = 0.8514$  and 0.8534 at  $\Delta t = 16.4$  yr (just before the peak in the He-energy release is reached) is represented by the dash-dotted line in Fig. 7. Since  $f_\sigma^{\text{CO}}$  barely exceeds 0.01, and the shell is still poor on  $^{12}\text{C}$ , the number of  $^{12}\text{C}+\alpha$  reactions is very low, and thus the ISCZ is enriched basically by  $^{12}\text{C}$ . Even at  $\Delta t = 20$  yr, shortly after the helium flash, when the ISCZ has already withdrawn from the nuclear active region, most of the energy is still produced in regions where  $f_\sigma^{\text{CO}}$  is less than 0.1 (dashed line). In the subsequent evolution the He burning region starts to contract, and the increasing density is further disfavouring the  $^{12}\text{C}+\alpha$  rate (compare, e.g., the  $\diamond$ 's on the dashed and solid line in Fig. 7).

However, with the decreasing He abundance and thus increasing C abundance the  $3\alpha$ -rate

$$r_{3\alpha} = n_{\text{He}}^3 \sigma_n^{3\alpha}$$

gradually weakens, while the opposite is true for the  $^{12}\text{C}+\alpha$ -rate

$$r_{\text{C}\alpha} = n_{\text{He}} n_{\text{C}} \sigma_n^{\text{C}\alpha},$$

despite the shell getting denser. Assuming, in a first approximation, that the burning shell consists only of  $\alpha$  and  $^{12}\text{C}$ , the minimum amount of He necessary to produce more C than O, can be determined (Fig. 8a) for different values of  $f_\sigma^{\text{CO}}$ . Following a shell in the He-burning region from  $\Delta t = 20$  yr onward, the reaction rate of  $^{12}\text{C}+\alpha$  becomes smaller (dotted line in Fig. 8a), and only small amounts of oxygen are fused (Fig. 8b). However, as soon as the helium abundance falls below a critical value (in this case  $Y \approx 0.2$ ),  $r_{\text{C}\alpha}$  increases considerably, and the oxygen mass fraction eventually reaches about 40%.

But this material remains inside the star and is never brought to the surface, as no ISCZ is apparent during the interpulse period, which could bridge the region between H- and He-burning shell.

In Fig. 6a the actual contribution of  $^{12}\text{C}(\alpha, \gamma)^{16}\text{O}$  to the He-burning reactions is shown, where

$$f_{\text{CO}} = \frac{r_{\text{C}\alpha}}{r_{3\alpha} + r_{\text{C}\alpha}}. \quad (3)$$

Clearly the scenario outlined before is visible. During the He shell flash  $3\alpha$  reactions are dominant over the whole burning region. Later, during quiescent He-burning, the outer shells in the burning regions still gain energy by the  $3\alpha$ -reaction, while in deeper layers, which have been processed previously by  $3\alpha$ , and thus are C-rich,  $^{12}\text{C}+\alpha$  provides the main energy source.

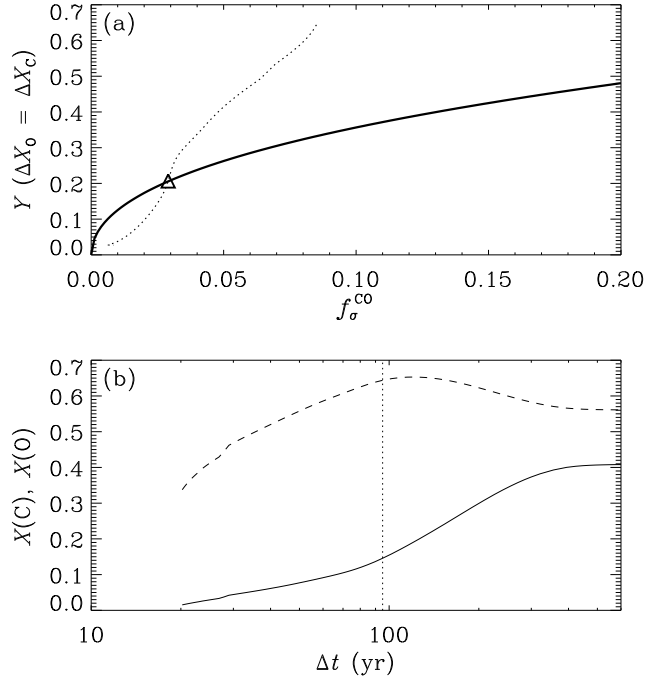


Figure 8. (a) The minimum helium mass fraction at which more C than O is produced for different values of the relative  $^{12}\text{C}+\alpha$  strength  $f_\sigma^{\text{CO}}$ . Above the solid line the carbon production is favoured. The dotted line indicated the evolution of the shell  $M_r/M_\odot = 0.8524$  from  $\Delta t = 20$  yr onward (from top to bottom). The triangle marks the position where O production starts to become dominant over C production. (b) The evolution of the C (dashed) and O (solid line) mass fractions within the same shell as in (a), where the dotted line indicates the moment denoted there by ‘ $\triangle$ ’.

### 3.2.2. Models with modified $3\alpha$ -rate

Modifying the  $0_2^+$  energy level of  $^{12}\text{C}$  effectively alters the temperature at which He-burning reactions ignite. In Fig. 9 the evolutions of  $5 M_\odot$  stars with  $\Delta E_R = -105, 0$  and  $+94$  keV, respectively are shown. Clearly the different moments of He-ignition are visible when the stars are crossing the Hertzsprung gap: the smaller the resonance energy the earlier the star stops its evolution toward the red and becomes bluer again. When its core He-supply is consumed, it eventually settles on the AGB.

Anyway the overall evolution of the star in the H-R diagram is only weakly modified by a different  $3\alpha$  reaction. But the altered He-burning temperature leads to a changed ratio of the  $^{12}\text{C}(\alpha, \gamma)^{16}\text{O}$ - to the  $3\alpha$ -rate. From Fig. 10 the strong sensitivity of the overall C and O production of a  $5 M_\odot$  star on  $E_R$  is apparent (dash-dotted line).

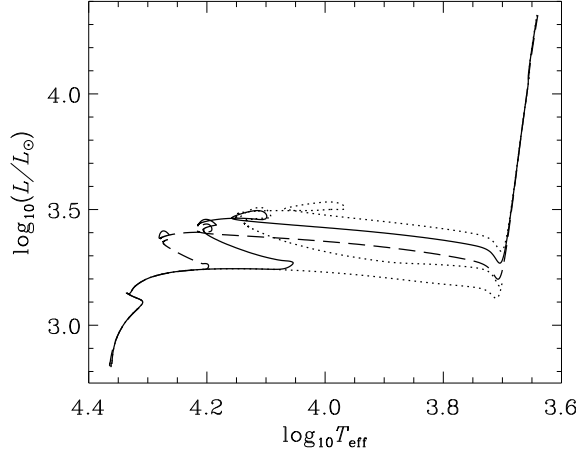


Figure 9. The evolution in the H-R diagram of models with different values of the  $0_2^+$  energy ( $E_R$ ) in  $^{12}\text{C}$ , where  $\Delta E_R = -105$  (dashed), 0 (solid) and  $+94\text{ keV}$  (dotted line). For the sake of clearance only the evolution until the beginning of the TP AGB is shown.

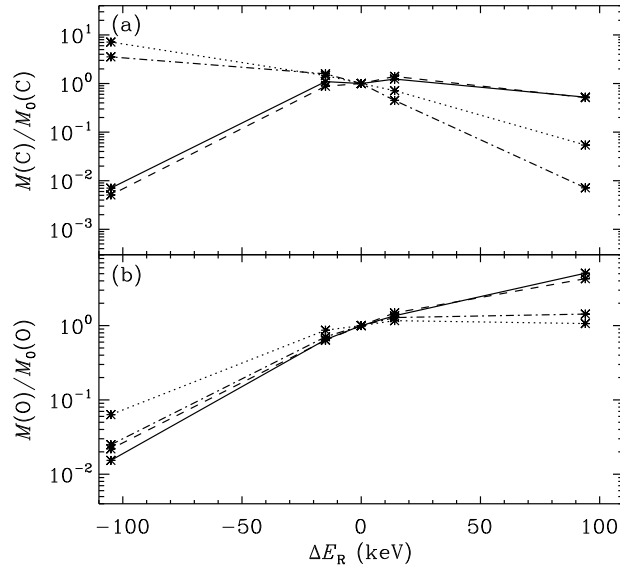


Figure 10. (a) The dependence of the C production on the  $0_2^+$  energy level relative to the standard case. The amount in the stellar wind is indicated by the dashed line, while the solid line represents the content in both envelope and wind. In addition, the complete amount of C created during the whole stellar lifetime (dash-dotted) and solely during the TP AGB (dotted line) are shown. The asterisks mark the actual models computed. (b) Like (a) but for oxygen.

Table IV. The C and O production of the  $5 M_{\odot}$  stars under scrutiny considering different stellar regions and/or phases.

$\Delta E_R$ keV	Summarized over whole star including the stellar wind whole lifetime		during TP AGB	
	$\frac{M(C)}{M_{\odot}}$	$\frac{M(O)}{M_{\odot}}$	$\frac{M(C)}{M_{\odot}}$	$\frac{M(O)}{M_{\odot}}$
-105	1.08	0.015	0.25	0.0019
-15	0.48	0.42	0.051	0.026
0	0.31	0.59	0.036	0.030
+14	0.14	0.76	0.025	0.035
+94	0.0022	0.84	0.0019	0.032

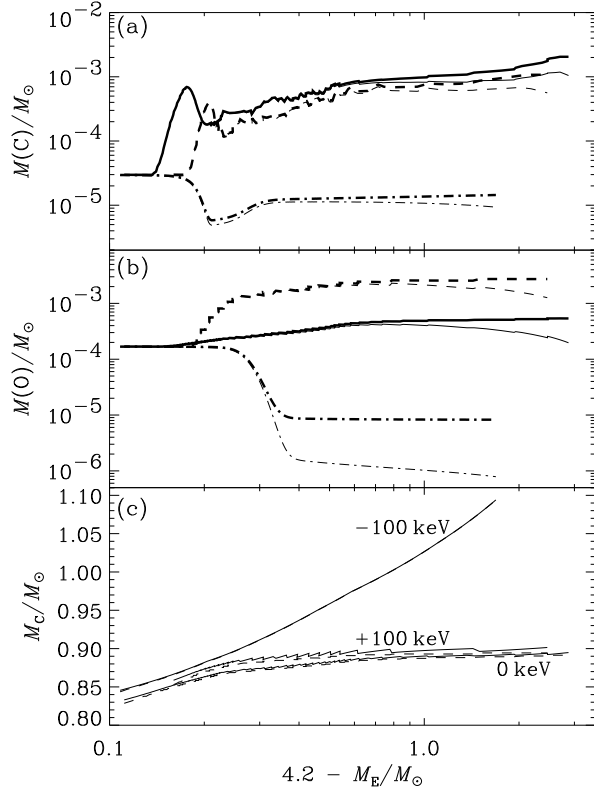
  

$\Delta E_R$ keV	Integrated over whole stellar lifetime			
	wind		envelope + wind	
$\frac{M(C)}{M_{\odot}}$	$\frac{M(O)}{M_{\odot}}$	$\frac{M(C)}{M_{\odot}}$	$\frac{M(O)}{M_{\odot}}$	
-105	$5.1 \times 10^{-6}$	$7.5 \times 10^{-6}$	$1.4 \times 10^{-5}$	$8.3 \times 10^{-6}$
-15	0.00088	0.00022	0.0022	0.00035
0	0.0010	0.00034	0.0021	0.00054
+14	0.0014	0.00051	0.0025	0.00073
+94	0.00051	0.0015	0.0011	0.0027

Changing the resonance energy by about  $\pm 100$  keV would yield a star consisting either completely of oxygen or of carbon (see also Table IV), which is similar to what have been found in Livio et al. (1989) and Paper I.

Almost the same tendency in the C and O production can be observed, if just the phase during the TP AGB is considered, although the suppression of the C-production is less pronounced. A completely different picture ensues, however, in particular for the C production, if only the abundances in the stellar wind or the stellar envelope are considered, which emerge through the 3<sup>rd</sup> dredge-up process. The carbon production is strongly suppressed when the resonance energy is lowered, and is still about 40% of the standard value even if  $\Delta E_R = 100$  keV, which is nearly opposite of what is expected.

A closer look reveals that the suppression of both the C and the O production for smaller values of  $E_R$  is caused by the weaker He-shell flashes. During the interpulse period usually the temperature in the He-burning shell decreases while the density increases. With reduced He-burning temperature the He shell does not contract as much as before and thus less energy is needed to re-establish thermally stable



*Figure 11.* (a) The C production during the TP AGB with decreasing envelope mass ( $M_E$ ) for a  $5 M_\odot$  model with  $\Delta E_R = +100$  (solid), 0 (dashed) and  $-100$  keV (dash-dotted line). The thick lines represent the total mass in wind and envelope, the thin lines solely the amount in the envelope. (b) Like (a) but for oxygen. (c) The evolution of the He- (solid) and C/O-core (dashed line) for the three cases.

conditions. The diminished energy release in the shell flash leads to a reduced ISCZ and later on to a smaller overlap of the convective envelope with regions previously occupied by the ISCZ. In fact, in the case of  $E_R = -100$  keV no ISCZ develops and thus no 3<sup>rd</sup> dredge-up occurs at all. The C and O abundances in the envelope are even smaller than initially due to CN and ON-conversions in the CNO-cycle when the convective envelope deepens along the RGB and later on the AGB (Fig. 11a,b).

However, the lack of a 3<sup>rd</sup> dredge-up maintains a metal-poor envelope and thus the star remains relatively hot. This inhibits the formation of dust-driven winds, and therefore results in a strongly reduced mass loss. In this case, the core mass can grow considerably larger than in models with standard  $3\alpha$  rates (cf. Fig. 11c). Although the  $5 M_\odot$

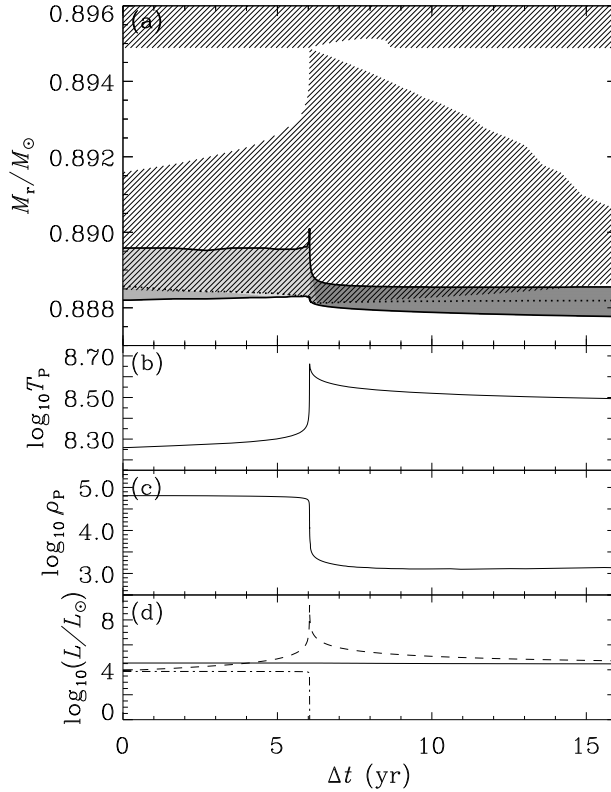


Figure 12. Like Fig. 6, but the  $0_2^+$  resonance of  $^{12}\text{C}$  has been increased by 94 keV.

star still remains below the Chandrasekhar limit, more massive stars probably get a too heavy core and cannot end up as a white dwarf. Thus the border between stars becoming white dwarfs and stars evolving further into a supernovae would be shifted significantly to lower masses. Since in supernova explosions also the deeper stellar layers would be slung into the ISM, the overall enrichment of the latter by C and O would be higher than in the case when the star creates C- and O-rich winds only via the 3<sup>rd</sup> dredge-up mechanism. For instance, the amount of oxygen produced in the star with  $E_R = -105$  keV solely during the TP AGB is  $8.6 \times 10^{-4} M_\odot$ , while in the standard case the wind and the envelope contain only  $6.6 \times 10^{-4} M_\odot$  (Table IV). Hence even in the case of a strongly reduced resonance energy, considerable amounts of O could still be created.

To understand the case of increased resonance energy the dredge-up process has to be examined thoroughly. In Fig. 12 the evolution during a selected thermal pulse in a model with  $\Delta E_R = +94$  keV is outlined. Due to the slightly modified lifetime of the star along the RGB and AGB

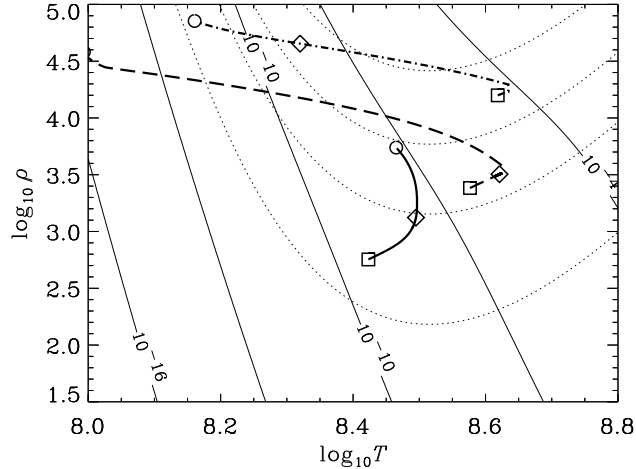


Figure 13. Like Fig. 7, but the  $0_2^+$  resonance of  $^{12}\text{C}$  has been increased by 100 keV. The dotted line mark the positions of  $f_{\sigma}^{\text{CO}} = 0.95, 0.67, 0.33$  and  $0.1$  (from bottom to top; Eq. (1)). The thick lines show the stratification of the shell with  $0.8877 < M_r/M_{\odot} < 0.8887$  at  $\Delta t = 6$  (dash-dotted),  $6.1$  (dashed) and  $15.5$  yr (solid line) (cf. Fig. 6). Equal symbols mark equal mass shells, where  $\square$ ,  $\diamond$  and  $\circ$  are located at  $M_r/M_{\odot} = 0.8877, 0.8882$  and  $0.8887$ , respectively.

the H- and He-burning shell are wider separated as in the standard case (compare Fig 6a and Fig. 12a). Nevertheless, the energy produced in the He-shell flash becomes higher, and the developing convective zone is still able to cover the whole H-devoid region between the shells. The main source of energy in the beginning of the shell flash remains the  $3\alpha$ -reaction (see dash-dotted line in Fig. 13), and thus still mainly carbon is produced. However, when the temperature and density are decreasing after the peak in  $L_{\text{He}}$ ,  $^{12}\text{C} + \alpha$  reactions considerably contribute to the energy generation and more oxygen than in the standard case is created (Fig. 12a).

Most of the energy is released around the maximum in  $L_{\text{He}}$  and therefore the bulk of the  $^{12}\text{C}$  and  $^{16}\text{O}$  nuclei are fused during a very short period ( $\lesssim 1$  yr). With the  $3\alpha$  reactions being still dominant in the early phases of the He-shell flash, considerable amounts of carbon can be produced. The withdrawing ISCZ carries  $^{12}\text{C}$  away from the nuclear active regions and saves it from being fused further as it happens in the He-burning shell. The subsequent 3<sup>rd</sup> dredge-up event enriches the surface with C and O, such that the final stellar envelope and wind still contain about 30–40% of the carbon mass compared to the case with unchanged resonance energy (Table IV).

In summary, the alternating phases of He-shell flash and quiescent He-burning during the TP AGB produce more C with respect to O than during the earlier phases (compare also the respective columns in Table IV). Moreover, the composition of the material enriching the envelope by the 3<sup>rd</sup> dredge-up has been processed nuclearly during the very short period of the He-shell flash, where the C/O-ratio is higher than in the intershell phase. To determine the C and O production of thermally pulsating stars and its dependence on the  $0_2^+$  energy level in  $^{12}\text{C}$ , it is hence crucial to follow accurately the He-shell flashes and the dredge-up events.

### 3.3. LOW-MASS STARS

We followed the evolution of a  $1.3 M_\odot$  star from the zero-age main sequence (ZAMS) through the He flash until the final thermal pulses on the AGB for the same values of the resonance energy as in the case of the  $5 M_\odot$  star. Certainly, the lifetime of these stars is too long to influence the yields in the early universe, but their C and/or O production might be important in anthropic reasonings for the fine-tuning of fundamental constants (see, e.g., Paper I).

Because of the smaller envelope mass of low-mass stars after the He-flash, the occurrence of the 3<sup>rd</sup> dredge-up is in this case much more sensitive to the amount of mass loss than in intermediate-mass stars. For instance, when using the same wind description like for the intermediate-mass stars, our low-mass stellar models did not show a 3<sup>rd</sup> dredge-up event. In this case, low-mass stars would not enrich the ISM with metals. However, observed C-enriched planetary nebulae with low-mass progenitors (see, e.g., Henry et al., 1996) show that the 3<sup>rd</sup> is operating in these stars. Therefore, we have chosen a reduced stellar wind, i.e., a pure Reimers' wind with efficiency parameter  $\eta = 0.25$ . With this description our  $1.3 M_\odot$  models have a few thermal pulses which become sufficiently strong to lead to 3<sup>rd</sup> dredge-up events.

#### 3.3.1. *The standard case*

In Fig. 14 the evolution of a  $1.3 M_\odot$  until the 3<sup>rd</sup> dredge-up on the TP AGB is shown. It should be noted that we detected a 2<sup>nd</sup> dredge-up before the star starts to pulsate thermally, which is, however, different from the standard 2<sup>nd</sup> dredge-up scenario of intermediate-mass stars: Toward the end of the horizontal-branch evolution the H-burning shell becomes considerably weaker. When the star ascends the AGB, H burning is re-ignited in a region of about  $0.02 M_\odot$  in width, which is much wider than the usual H-shell burning size of less than  $0.001 M_\odot$  during the late RGB or during the TP AGB. Although the H-burning

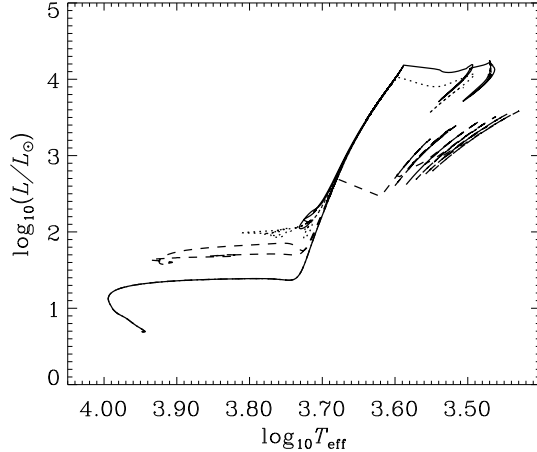


Figure 14. The evolution of  $1.3 M_{\odot}$  stars with  $\Delta E_R = -105$  (dashed), 0 (dotted) and  $+94 \text{ keV}$  (solid line) in the H-R diagram.

shell rapidly becomes narrower, the established He profile remains in regions above this shell, like during the early RGB. In the subsequent evolution the convective envelope deepens and reaches the outer tail of that He profile, hence increasing the mass fraction of He on the surface by about 0.002. The surface distribution of the CNO-elements is unaltered, i.e., remains the same as after the 1<sup>st</sup> dredge-up on the RGB.

This 2<sup>nd</sup> dredge-up is thus in contrast to the 2<sup>nd</sup> dredge-up in intermediate-mass stars, where the convective envelope deepens into the region of the H-burning shell, which is not active during this event. In low-mass stars the H-burning shell is active, but the envelope reaches areas, where a He profile was left over by a previously wider H-burning region. In this sense, the mechanism of the 2<sup>nd</sup> dredge-up in low-mass stars is similar to the 1<sup>st</sup> dredge-up. This assessment is further supported by the unaltered surface CNO distribution, which shows that the H-burning conditions in the areas engulfed by the growing convective envelope have been similar to the conditions at the sub-giant branch.

During the 4<sup>th</sup> thermal pulse the He shell flashes are strong enough to cause the envelope convective zone to penetrate regions which were previously occupied by the IS CZ, i.e., a 3<sup>rd</sup> dredge-up event occurs. With our mass-loss description only 2 further thermal pulses take place until the envelope mass has become less than about  $10^{-3} M_{\odot}$ , and the star evolves into the planetary-nebulae phase and beyond. The enrichment of the surface with C and O is not altered considerably during the subsequent 3<sup>rd</sup> dredge-up events.

Table V. The C and O production of the  $1.3 M_{\odot}$  stars under scrutiny considering different stellar regions and/or phases.

$\Delta E_R$ keV	Summarized over whole star including the stellar wind			
	whole lifetime		during TP AGB	
	$\frac{M(C)}{M_{\odot}}$	$\frac{M(O)}{M_{\odot}}$	$\frac{M(C)}{M_{\odot}}$	$\frac{M(O)}{M_{\odot}}$
-105	0.43	0.0030	0.088	0.00053
-15	0.30	0.25	0.028	0.012
0	0.21	0.38	0.036	0.029
+14	0.11	0.51	0.028	0.036
+94	0.0035	0.66	0.0031	0.073

$\Delta E_R$ keV	Integrated over whole stellar lifetime			
	wind		envelope + wind	
	$\frac{M(C)}{M_{\odot}}$	$\frac{M(O)}{M_{\odot}}$	$\frac{M(C)}{M_{\odot}}$	$\frac{M(O)}{M_{\odot}}$
-105	0.013	$4.8 \times 10^{-5}$	0.025	$9.4 \times 10^{-5}$
-15	0.0011	$2.6 \times 10^{-5}$	0.0050	$9.6 \times 10^{-5}$
0	0.00072	$3.1 \times 10^{-5}$	0.0035	0.00011
+14	0.0011	$6.7 \times 10^{-5}$	0.0048	0.00022
+94	0.00033	0.00022	0.00093	0.00061

### 3.3.2. Models with modified $3\alpha$ -rate

The different He-burning temperatures in the models with modified  $3\alpha$  rate have various consequences on the evolution of low-mass stars. The luminosity of the HB and of the AGB is reduced when lowering  $E_R$  due to the earlier onset of He-burning (Fig. 14). In this case, a stronger H-burning shell relative to the He-burning core leads in addition to a more extended blue loop on the HB. (Note that metal-poor stars also have a more extended blue loop than their metal-rich counterparts because of their stronger H-burning shell.) For higher values of  $E_R$  the opposite behaviour can be observed.

The effect of the modified  $3\alpha$ -rate on the C and O production is as expected: the lower the resonance energy, the higher the C and the lower the O production rate (Fig. 15). Since the mechanism of the thermal pulses is the same as in the  $5 M_{\odot}$  star, a smaller sensitivity on  $E_R$  is obtained also for the low-mass stars when considering the detailed  $3^{\text{rd}}$  dredge-up process. However, in contrast to the  $5 M_{\odot}$  star, the  $1.3 M_{\odot}$  model with  $\Delta E_R = -105$  still shows a  $3^{\text{rd}}$  dredge-up. The reason is the stronger degeneracy of the C/O core in the low-mass stars which leads to more energetic He-shell flashes.

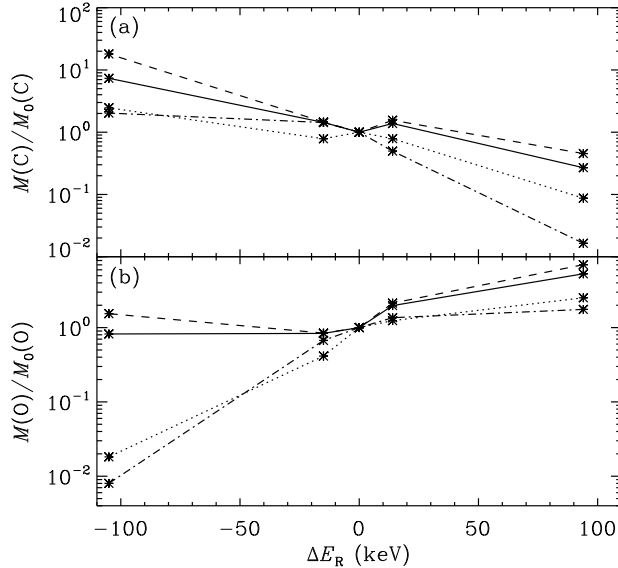


Figure 15. The dependence of the C (a) and O (b) production on the  $0_2^+$  energy level relative to the standard case. The line-styles correspond to Fig. 10.

It should be noted that the longer lifetime of the model with lowered resonance energy on the TP AGB, and the hence higher number of pulses, compensate for the reduced O production per pulse. Overall the O yield appears to be quite insensitive to moderate reductions of the resonance energy. However, the total amount of O produced in these stars is about an order of magnitude smaller than the C yields, and its present contribution to the overall amount of O in the ISM is negligible. Nevertheless, the much higher number of low-mass compared to intermediate-mass and massive stars might still produce noticeable amounts of oxygen after a few billion years, and thus would considerably enrich the ISM at a later time.

#### 4. Conclusions

We have provided an improved determination of the dependence of the C and O production in low-, intermediate-mass, and massive stars on the  $0_2^+$  resonance energy. Our results show that the C and O production in massive stars is depending on the initial stellar mass, and overall somewhat smaller than estimated in our previous work (Paper I). The basic reasons for the different findings are thought to be the different

Table VI. The relative change in the ratio of  $M_{\text{SN}}(\text{C})$  to  $M_{\text{SN}}(\text{O})$  ('C/O-ratio') in the massive stars of Table I compared to the standard case ( $\Delta E_{\text{R}} = 0$ ).

$\frac{\Delta E_{\text{R}}}{\text{keV}}$	$15 M_{\odot}$	$25 M_{\odot}$
-100	33	28
0	1	1
+100	0.34	0.11

treatment of semiconvection and/or the different  $^{12}\text{C}(\alpha, \gamma)^{16}\text{O}$  reaction rate.

Massive stars are the primary source of nucleosynthesis in the early universe, and thus their yields are mainly determining the C and O content in very metal-poor stars. With a different  $3\alpha$  rate caused in the early universe, e.g., by a variant fine-structure constant, in particular the C/O ratio would be different than in standard galacto-chemical models. Presently, those standard models are, however, able to reproduce the observed abundances pretty well, although an uncertainty of about 50% in the theoretical yields at very low metallicities is apparent (see, e.g., Liang et al., 2001, for an overview). In Table VI the relative changes of the final C/O ratios for  $\Delta E_{\text{R}} = \pm 100 \text{ keV}$  compared to the standard case are provided for our massive star models. A coarse limit on the variations of  $\Delta E_{\text{R}}$  can be obtained by not allowing the change in the C/O ratio in those stars to become larger than the error in the standard yields of about 50%. By linearly interpolating the results of Table VI  $\Delta E_{\text{R}}$  is constrained to be between about -5 and +50 keV. Hence, any possible change in a fundamental constant which causes a shift in  $E_{\text{R}}$  larger than this would hardly be consistent with the observations. For a more accurate determination of the allowed values of  $\Delta E_{\text{R}}$  more models with different  $\Delta E_{\text{R}}$  and different masses would be necessary, and their yields have to be folded by an initial mass function to obtain an average value.

More stringent constraints neither can be obtained from the intermediate-mass stars, as we have found that the sensitivity of their C and O production is considerably smaller than claimed in our previous work. In Paper I the C and O yields in low- and intermediate-mass stars have been obtained by determining the abundances within the He-burning shell *after* the 3<sup>rd</sup> thermal pulse. Clearly, by that method the suppression of the carbon production for  $\Delta E_{\text{R}} > 0$  is strongly overestimated, as much more C is produced during the He-shell flash.

Only during this small period an ISCZ exists by which C- and O-rich material is brought close to the H-rich convective envelope, which in the ensuing evolution deepens and thus enriches the surface by He-burned material.

For lower resonance energies the situation is even more involved. The diminishing extent of the ISCZ and the thus strongly reduced dredge-up for  $\Delta E_R < 0$  causes a strong reduction of the C *and* O enrichment of the envelope. However, the consequent smaller mass-loss rates enable the creation of a much heavier C/O core, which could cause stars to explode as a supernova which much smaller initial mass than in the standard case. More C and O rich material would be blown into the ISM than by stellar winds in TP AGB stars. Thus even for  $\Delta E_R < 0$  the absolute oxygen mass in the ISM would still be significant, although its relative abundance compared to carbon would still be small. To examine this more thoroughly, population-synthesis computations would be necessary, which are, however, beyond the aim of the present work.

In low-mass stars the 3<sup>rd</sup> dredge-up is never suppressed for the variations of  $\Delta E_R$  considered in this work. Moreover, the higher number of thermal pulses in the case of  $\Delta E_R < 0$  almost compensates for the reduced efficiency in the O production per pulse. However, the oxygen yields of low-mass stars are very small, and they would not contribute noticeably to the O enrichment of the ISM for many billion years.

Summarising, when considering the full stellar evolution especially for low- and intermediate-mass stars the fine tuning with respect to the obtained carbon and oxygen abundance is more complicated and far less spectacular than we found in Paper I. Therefore, the results obtained in this work could reduce the anthropic significance of the  $3\alpha$  process considerably.

### Acknowledgements

This work was promoted by the John Templeton Foundation (938-COS153). H.S. has been supported by a Marie Curie Fellowship of the European Community programme ‘Human Potential’ under contract number HPMF-CT-2000-00951, and A.H., in part, by the Department of Energy under grant B341495 to the Center for Astrophysical Thermonuclear Flashes at the University of Chicago, and a Fermi Fellowship at the University of Chicago. T.R. acknowledges a PROFIL professorship from the Swiss National Science foundation (grant 2024-067428.01) and the support from the Swiss NSF (2000-061031.02). A.C. was supported by OTKA-T037548/FKFP-0147-2001.

## References

Adelberger, E. G., S. M. Austin, J. N. Bahcall, A. B. Balantekin, G. Bogaert, et al.: 1998. *Rev. Mod. Phys.* **70**, 1265.

Alexander, D. R. and J. W. Fergusson: 1994. *ApJ* **437**, 879.

Böhm-Vitense, E.: 1958. *Z. Astrophys.* **46**, 108.

Buchmann, L.: 1996. *ApJ* **468**, 127.

Calmet, X. and H. Fritsch: 2002. *Eur. Phys. J. C* **24**, 639.

Cassisi, S., M. Salaris, and A. W. Irwin: 2003a. *ApJ* **588**, 862.

Cassisi, S., H. Schlattl, M. Salaris, and A. Weiss: 2003b. *ApJ* **582**, L43.

Caughlan, G. R., W. A. Fowler, M. J. Harris, and B. A. Zimmerman: 1985. *Atomic Data Nuc. Data Tables* **32**, 197.

Chacko, Z., C. Grojean, and M. Perelstein: 2002, 'Fine Structure Constant Variation from a Late Phase Transition'. Saclay T02/038, hep-ph/0204142.

Cook, C. W., W. A. Fowler, C. C. Lauritsen, and T. Lauritsen: 1957. *Phys. Rev.* **107**, 508.

Dent, T. and M. Fairbairn: 2003. *Nucl. Phys. B* **653**, 256.

Faulkner, D. J.: 1970. *ApJ* **162**, 513.

Finzi, A. and R. A. Wolf: 1971. *A&A* **11**, 418.

Fiorentini, G. and B. Ricci: 2002. In: *Proc. of ESO-CERN-ESA Symposium on Astronomy, Cosmology and Fundamental Physics, Garching, Germany, 4-7 March 2002*.

Firestone, R. B., V. S. Shirley, C. M. Baglin, S. Y. F. Chu, and J. Zipkin: 1996, *Table of Isotopes*. New York: John Wiley & Sons, Inc., eighth edition.

Heger, A., N. Langer, and S. E. Woosley: 2000. *ApJ* **528**, 368.

Heger, A., S. E. Woosley, T. Rauscher, R. D. Hoffman, and M. M. Boyes: 2002. *New Astron. Rev.* **46**, 463.

Henry, R. B. C., K. B. Kwitter, and J. W. Howard: 1996. *ApJ* **458**, 215.

Hoyle, F.: 1954. *ApJS* **1**, 121.

Hoyle, F., D. N. F. Dunbar, W. A. Wenzel, and W. Whaling: 1953. *Phys. Rev.* **92**, 1095.

Iglesias, C. A. and F. J. Rogers: 1996. *ApJ* **464**, 943.

Janka, H.-T., R. Buras, K. Kifonidis, M. Rampp, and T. Plewa: 2002. In: W. Hillebrandt and B. Leibundgut (eds.): *From Twilight to Highlight: The Physics of Supernovae*. Berlin: Springer Verlag, in press.

Kippenhahn, R. and A. Weigert: 1990, *Stellar Structure and Evolution*. Berlin, Heidelberg: Springer-Verlag.

Kunz, R., M. Fey, M. Jaeger, A. Mayer, J. W. Hammer, et al.: 2002. *ApJ* **567**, 643.

Kunz, R., M. Jaeger, A. Mayer, J. W. Hammer, G. Staudt, et al.: 2001. *Phys. Rev. Lett.* **86**, 3244.

Langacker, P., G. Segre, and M. J. Strassler: 2002. *Phys. Lett. B* **528**, 121.

Langer, N., M. El Eid, and K. J. Fricke: 1985. *A&A* **145**, 179.

Liang, Y. C., G. Zhao, and J. R. Shi: 2001. *A&A* **374**, 936.

Limongi, M., O. Straniero, and A. Chieffi: 2000. *ApJS* **129**, 625.

Livio, M., D. Hollowell, A. Weiss, and J. W. Truran: 1989. *Nature* **340**, 281.

Marigo, P., A. Bressan, and C. Chiosi: 1996. *A&A* **313**, 545.

Murphy, M. T., J. K. Webb, V. V. Flambaum, M. J. Drinkwater, F. Combes, and T. Wiklind: 2001. *MNRAS* **327**, 1244.

Nieuwenhuijzen, H. and C. de Jager: 1990. *A&A* **231**, 134.

Oberhummer, H., A. Csótó, M. Fairbairn, H. Schlattl, and M. M. Sharma: 2003. *Nucl. Phys. A* **719**, 283c.

Oberhummer, H., A. Csótó, and H. Schlattl: 2000. *Sci* **289**, 88.

Rauscher, T., A. Heger, R. D. Hoffman, and S. E. Woosley: 2002. *ApJ* **576**, 323.

Reimers, D.: 1975. *Mem. Soc. Roy. Sci. Liège* **8**, 369.

Rogers, F. J., F. J. Swenson, and C. A. Iglesias: 1996. *ApJ* **456**, 902.

Schlattl, H.: 1999. Ph.D. thesis, Technical University Munich.

Schlattl, H.: 2002. *A&A* **395**, 85.

Schlattl, H., S. Cassisi, M. Salaris, and A. Weiss: 2001. *ApJ* **559**, 1082.

Vassiliadis, E. and P. R. Wood: 1993. *ApJ* **413**, 641.

Wagenhuber, J. and A. Weiss: 1994. *A&A* **286**, 121.

Weaver, T. A. and S. E. Woosley: 1993. *Phys. Rept.* **227**, 65.

Weaver, T. A., G. B. Zimmerman, and S. E. Woosley: 1978. *ApJ* **225**, 1021.

Weiss, A. and H. Schlattl: 2000. *A&AS* **144**, 487.

Wood, P. R. and D. J. Faulkner: 1986. *ApJ* **307**, 659.

Woosley, S. E., A. Heger, T. Rauscher, and R. D. Hoffman: 2003. *Nucl. Phys. A* accepted.

Woosley, S. E., A. Heger, and T. A. Weaver: 2002. *Rev. Mod. Phys.* **74**, 1015.

Woosley, S. E. and T. A. Weaver: 1995. *ApJS* **101**, 181.

